sustainability

MDPI

Article

A High-Temperature Risk Assessment Model for Maize Based on MODIS LST

Xinlei Hu [1,2], Zuliang Zhao [1,2], Lin Zhang [1,2], Zhe Liu [1,2,*], Shaoming Li [1,2] and Xiaodong Zhang [1,2]

1 College of Land Science and Technology, China Agricultural University, Beijing 100083, China; huxinlei@cau.edu.cn (X.H.); zlzhao@cau.edu.cn (Z.Z.); linzhangcau@cau.edu.cn (L.Z.); lishaoming@cau.edu.cn (S.L.); zhangxd@cau.edu.cn (X.Z.)

2 Key Laboratory of Remote Sensing for Agri-Hazards, Ministry of Agriculture and Rural Affairs, Beijing 100083, China

* Correspondence: liuz@cau.edu.cn; Tel.: +86-010-627-37554

Received: 13 October 2019; Accepted: 20 November 2019; Published: 22 November 2019



Abstract: Currently, high-temperature risk assessments of crops at the regional scale are usually conducted by comparing the observed air temperature at ground stations or via the remote sensing inversion of canopy temperature (such as MODIS (moderate-resolution imaging spectroradiometer) land surface temperature (LST)) with the threshold temperature of the crop. Since this threshold is based on the absolute temperature value, it is difficult to account for changes in environmental conditions and crop canopy information between different regions and different years in the evaluation model. In this study, MODIS LST products were used to establish an evaluation model (spatiotemporal deviation mean (STDM)) and a classification method to determine maize-growing areas at risk of high temperatures at the regional scale. The study area was the Huang-Huai-Hai River plain of China where maize is grown and high temperatures occur frequently. The spatiotemporal distribution of the high-temperature risk of summer maize was determined in the study area from 2003 to 2018. The results demonstrate the applicability of the model at the regional scale. The distribution of high-temperature risk in the Huang-Huai-Hai region was consistent with the actual temperature measurements. The temperatures in the northwestern, southwestern, and southern parts were relatively high and the area was classified as a stable zone. Shijiazhuang, Jiaozuo, Weinan, Xi'an, and Xianyang city were located in a zone of increasing high temperatures. The regions with a stable high-temperature risk were Xiangfan, Yuncheng, and Luoyang city. Areas of decreasing high temperatures were Handan, Xingtai, Bozhou, Fuyang, Nanyang, Linfen, and Pingdingshan city. Areas that need to focus on preventing high-temperature risks include Luoyang, Yuncheng, Xianyang, Weinan, and Xi'an city. This study provides a new method for the detailed evaluation of regional high-temperature risk and data support.

Keywords: MODIS LST; spatiotemporal deviation; high-temperature risk; maize

1. Introduction

Maize is a thermophilic crop, but high temperatures have an adverse impact on its growth and development [1–5]. Climate change has aggravated the risk of high temperatures in temperate regions. For example, China's Huang-Huai-Hai summer maize planting area has suffered a large-scale reduction due to the decline in corn pollen viability from high temperatures (>34 °C) in the flowering period from 2013 to 2018. The poor resistance of existing maize varieties in this region and inadequate knowledge of farmers and agricultural departments pertaining to the location of high risk areas and the occurrence of high temperatures have led to the failure to implement timely risk reduction measures in many areas,

thereby resulting in low maize production in many areas [3,4]. The high-temperature risk assessment of crops is a research topic with broad and current interest.

At present, there are three main research methods that have been used to assess the spatiotemporal distribution of the high-temperature risk of crops at the regional scale: (1) The interpolation of temperature data obtained from meteorological stations; (2) the surface temperature inversions using remote sensing data; (3) regression methods based on surface temperature inversion.

In the temperature interpolation method, the temperature threshold of the crop is the atmospheric temperature threshold (i.e., 34 °C for maize in the flowering period) and it can be directly determined whether there is a high-temperature risk based on observations obtained from meteorological stations. The regional distribution of high-temperature risks is obtained by performing spatial interpolation of the temperature data at meteorological stations. For example, Liu [6] investigated the spatial distribution of high-temperature heat damage during the flowering period of maize in Huang-Huai-Hai using temperature data obtained from meteorological stations. Liang et al. [7] explored the temporal and spatial variation trends and extreme probability distribution of the high-temperature heat damage of early rice in China using meteorological temperature data. Meteorological stations provide accurate and near-real-time point-based temperature data. However, due to the limited number of meteorological stations and terrain influences, the observed temperature data only represent local conditions for a small region. At the regional scale, such as the Huang-Huai-Hai summer maize planting area, the interpolated data have low precision, and their ability to describe spatial heterogeneity over a wide range of temperatures is limited, especially their ability to assess high temperatures [8,9]. Moreover, most meteorological stations are located near urban areas, while agricultural areas are poorly represented.

The surface temperature inversion method based on remote sensing data is based on the principle of thermal radiation and reflection and the infrared band of remote sensing images is used to calculate the surface temperature. The split window method is used to retrieve the land surface temperature (LST) based on differential water vapor absorption in two adjacent infrared channels [10]. The basis of the split window algorithm is that the radiance attenuation for atmospheric absorption is proportional to the radiance difference of simultaneous measurements at two different wavelengths, each subject to different amounts of atmospheric absorption [11].Generally, split-window and daytime/nighttime land surface temperature (LST) algorithms are used to calculate the surface temperature [12,13]; the inversion parameters are adjusted according to land use/cover, surface moisture, roughness, and viewing angles [14]. Ri [15] proposed an improved surface temperature inversion algorithm based on Terra/MODIS LST data and observed an improvement in inversion accuracy. Wang and He [16] improved the split-window algorithm to ensure that the inversion temperature data were consistent with the land use type of agricultural areas to improve the accuracy of the results for agricultural applications. Surface temperature data based on remote sensing images have the characteristics of large-scale continuity and high temporal resolution. However, the thermal infrared band of remote sensing images is affected by atmospheric conditions, especially during rainy summers, and extensive cloud cover will lead to missing values in the images [17,18]. In addition, the surface temperature is not equal to the atmospheric temperature, and an atmospheric temperature threshold cannot be used to identify a high-temperature risk.

In the regression method based on surface inversion products, a relationship is established between LST and meteorological temperature data; this method has been used for regional temperature risk assessment. Zhu et al. [19] used MODIS LST data to estimate the daily maximum and minimum temperatures. Huang et al. [20] estimated the daily average temperature based on MODIS LST data and conducted spatiotemporal interpolation to create a spatially continuous daily average temperature map. The combination of remote sensing data and meteorological data has been used to obtain regional-scale temperature distribution maps with high spatial resolution. However, for large-scale and inter-annual high-temperature risk assessment research, the relationship between surface temperatures

and atmospheric temperatures needs to be repeatedly calibrated due to complex and variable crop canopy information and environmental factors such as light, temperature, and moisture [21].

Current regional-scale high-temperature risk assessment methods (such as killing degree days model [22,23]) commonly focus on the absolute temperature threshold for crop growth, calculate the temperature at each location, or use inversion methods to determine the temperature based on ground temperatures (such as MODIS LST). MODIS LST data represent the temperature of the land surface [24], while the meteorological temperature are point-based data of the atmospheric temperature at 1.5 m above ground. Therefore, a discrepancy exists between the MODIS LST and the temperature of the meteorological stations [25,26]. Moreover, the meteorological temperatures cannot be used to determine the threshold for high-temperature risk assessment based on remote sensing data. Moreover, repeated calibrations are required when using the temperature regression method based on surface inversion products for large-scale and inter-annual analysis [25,27,28].

Data inversion and risk assessment based on the absolute temperature threshold are hampered by complex and ever-changing environmental factors and crop canopy conditions [29]. Environmental and crop impacts can be considered as systematic errors in the same ecological zone. If this systematic error is uniformly eliminated, the modified temperature (i.e., the relative surface temperature rather than the absolute temperature) of each spatial unit in the respective ecological zone can be used to determine high- or low-temperature risks, and repeated calibrations are not required. High-temperature risk of Huang-Huai-Hai summer maize region in China usually happens in July–August. The deviation between the inversion temperature of each spatial unit and the regional mean during this time can be used to express the risk of high temperature.

In this study, we focused on the Huang-Huai-Hai summer maize region in China and used MODIS LST products to develop a relative high-temperature risk assessment model and hierarchical classification method, based on which, we explored the changes of regional relative high temperatures during 2003–2018.

2. Materials and Methods

2.1. Study Area

The study area, Huang-Huai-Hai summer maize region, is located in North China plain (31 to 40° N and 107 to 123° E), including the Shandong and Henan provinces, most of Beijing, Tianjin, and Hebei, the southern regions of Shanxi and Shaanxi, and the northern regions of Jiangsu, Anhui, and Hubei [2,30,31] (Figure 1). The Huang-Huai-Hai summer maize region is one of the largest maize-producing areas in China. There are four distinct seasons and the same number of periods for rain and heat. The annual solar radiation is 4605–5860 MJ/m^2, the annual sunshine hours are 2300–2800 h, the annual average temperature is 10–15 °C, the average summer temperature is 28–32 °C, and the accumulated temperature of ≥10 °C for the whole year is 3600–4900 °C. Rainfall is relatively abundant but occurs mainly in the summer. The rainfall in July and August accounts for more than 70% of annual rainfall and is characterized by high rainfall concentration, high temperatures, and large evaporation [32].

The land cover types of the study area generated from the Collections 5.1 MODIS land cover type product MCD12Q1 [33,34] and maize cropland data are shown in Figure 1. Only six general land cover classes are displayed in Figure 1. This area is mainly dominated by cropland, urban, and woodland. In the study area, there are 79 national meteorological observation stations, which is inadequate for an area of about 700,000 km^2. In terms of spatial distribution, these meteorological stations are mostly distributed near towns (Figure 1), which means that they are relatively weak in representing farmland temperatures.

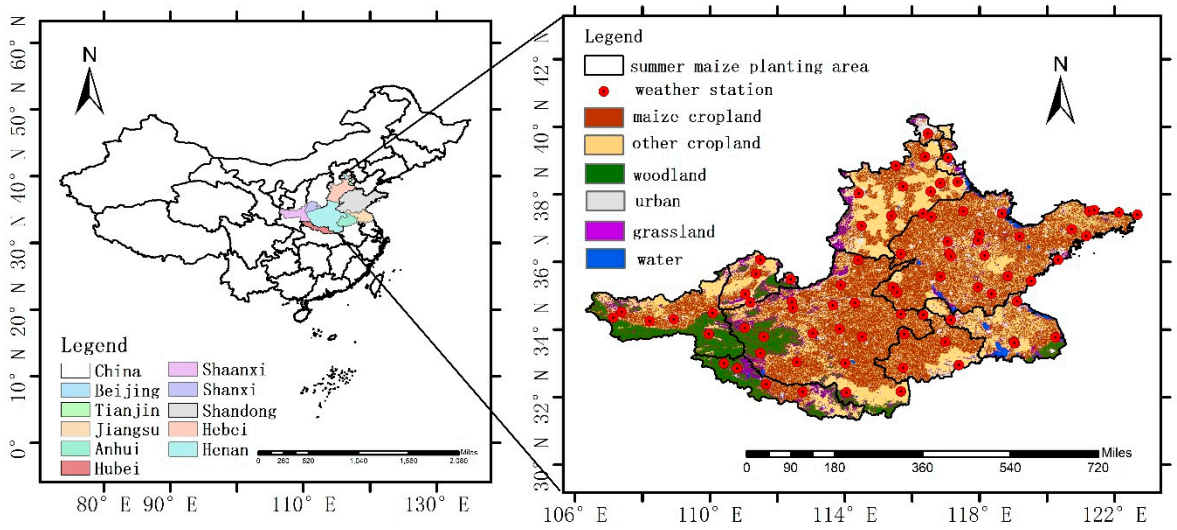


Figure 1. Study area.

2.2. Data Source

The MYD11A1 product, which is the L3 LST product (V006 version), was derived from the daily LST data provided by the MODIS sensor on the AQUA satellite and was downloaded from the Land Processes Distributed Active Archive Center (LP DAAC) website. The characteristics of the MYD11A1 product are shown in Table 1.

Table 1. Introduction of the characteristics of MYD11A1 remote sensing products.

Characteristic	Description
Collection	Aqua MODIS
File Size	~2 MB
Temporal Resolution	Daily
Temporal Extent	2002-07-04 to Present
Spatial Extent	Global
Coordinate System	Sinusoidal
File Format	HDF-EOS
Geographic Dimensions	1200 km × 1200 km
Number of Science Dataset (SDS) Layers	12
Columns/Rows	1200 × 1200
Pixel Size	1000 m

The period during which corn is susceptible to high temperatures extends from July to August when flowering and filling occur [35]. During the flowering period, high temperatures affect the pollen activity of corn, which in turn affects fruiting [36,37]. In the grain filling period [38], high temperatures result in accelerated physiological and biochemical reaction rates of maize, which leads to a shortening of the filling period, which affects the dry matter accumulation of maize [29,38,39]. Therefore, we used the MYD11A1 product from July to August of 2003–2018. The product is based on the split-window algorithm using the thermal infrared bands 31 (10.78–11.28 m) and 32 (11.77–12.27 m) [40]. The temporal resolution is 1 d and the spatial resolution is 1 km. The images are stored in the HDF format, and the image size is 1200 (rows) × 1200 (columns); a total of 12 sub-datasets were used. There exists 2 LST data records per day, which pass over the study site (local solar time), mostly around 1:30 am and 13:30 pm. These times are relatively close to the times of the maximum and minimum temperature daily data. The introduction of each band of MYD11A1 is shown in Table 2. In order to completely cover the Huang-Huai-Hai summer maize region, we used four daily remote sensing images (h26v04, h26v05, h27v05, and h28v05). In total, 3968 images were used for the study period (2003–2018).

Table 2. Introduction of each band of MYD11A1 remote sensing products.

Name	Units	Description
LST_Day_1km	K	Daily daytime land-surface temperature at 1 km grids
QC_Day	*	Daytime LST quality indicators for 1 km L3 LST
Day_view_time	h	Local sun time of daytime land-surface temperature observation
Day_view_angl	deg	View zenith angle of daytime land-surface temperature
LST_Night_1km	K	Daily nighttime 1 km grid land-surface temperature
QC_Night	*	Nighttime LST quality indicators for 1 km L3 LST
Night_view_time	h	Local sun time of nighttime land-surface temperature observation
Night_view_angl	deg	View zenith angle of nighttime land-surface temperature
Emis_31	*	Band 31 emissivity
Emis_32	*	Band 32 emissivity
Clear_day_cov	*	day clear-sky coverage of the LST observation
Clear_night_cov	*	night clear-sky coverage of the LST observation

The maize cultivated land data were derived from the statistical data of the second survey of national cultivated land in 2013 [41]. This is a raster dataset with a resolution of 1 km. The use of a mask of cultivated land data in the MODIS LST image reduces the influence of non-cultivated land factors on the model and improves the accuracy of the results. The administrative boundary data and digital elevation model (DEM) were obtained from the Resource and Environment Data Cloud Platform (http://www.resdc.cn/Datalist1.aspx?FieldTyepID=9, 13).

2.3. Data Preprocessing

The geospatial data abstraction library (GDAL) was used for data preprocessing. Two steps were used for the preprocessing of cultivated land data. First, the cultivated land data were resampled using the nearest-neighbor method in ArcMap to obtain faster data at the same resolution (1 km) as the MODIS LST. Then, the cultivated land data were cropped to match the Huang-Huai-Hai summer maize region. The coordinate system was WGS-84.

Four steps were used for LST data preprocessing. First, we extracted the corresponding bands of the MYD11A1 (LST_Day_1 km, LST_Night_1 km). Next, we spliced the four LST products covering the study area (h26v04, h26v05, h27v04, and h27v05) and projected them to the WGS-84 coordinate system. We masked the output using the Huang-Huai-Hai area layer. Finally, we used the following formula to convert the LST value from Kelvin to Celsius:

$$c = 0.02\,\mathrm{T} - 273.15, \quad (1)$$

where c is the temperature in Celsius temperature, T is the absolute temperature, and 0.02 is the scale factor.

2.4. Relative High Temperature Risk Assessment Model

As described in the introduction, we cannot directly use the meteorological temperature threshold in the models built based on LST data. Moreover, the research goal of this paper is to construct a spatial distribution model for regional relative high temperature risk analysis, rather than the thermal damage effects caused by high temperature. Since high temperatures during the day and at night inhibit the growth of maize [35,42–44], in order to comprehensively consider the high temperature effects of day and night, and to quantify the relative high temperature risk of each spatial unit within a given region and its spatio-temporal differences, we designed a spatio-temporal deviation mean

(STDM) model based on LST data. The modeling process is shown in Figure 2. First, the average daily temperature in the study area was used as a benchmark, as shown in Equation (2). Then, the original value in each cell was replaced by the deviation of the LST value from the daily mean temperature, as shown in Equation (3). Next, Equation (4) is used to calculate the average deviation of these two periods, describing the effects of day and night high temperatures to provide an accurate estimate of the high temperature risk of maize. Finally, due to the large spatial and temporal scale of this study, there is a data imbalance problem. In order to minimize this imbalance, we propose a pixel-by-pixel calculation of the effective value in the region, as shown in Equation (5).

$$\overline{\mathrm{x}} = \frac{\sum_{k=1}^{N} x_i}{N}, \tag{2}$$

where x_i is the value of the non-null pixels, N is the number of non-null pixels, and $\overline{\mathrm{x}}$ is the mean of the non-null pixels, i.e., the average temperature of the region.

$$\mathrm{bias}_t = x_i - \overline{\mathrm{x}}, \tag{3}$$

where bias_t is the regional spatial deviation value of the non-null pixels at time t.

$$\begin{cases} \mathrm{bias_{day}} = \mathrm{x_i} - \overline{\mathrm{x}}(t = 13:30) \\ \mathrm{bias_{night}} = \mathrm{x_i} - \overline{\mathrm{x}}(t = 1:30) \\ \mathrm{bias_{ht}} = \frac{(\mathrm{bias_{day}} + \mathrm{bias_{night}})}{\mathrm{n}}(n = 1, 2) \end{cases} \tag{4}$$

where bias_{day} and bias_{night} are the regional spatial deviation values of the non-null pixels in the image at 1:30 pm and 1:30 am, respectively and n is the number of valid values of bias_{day} and bias_{night} in the corresponding spatial positions in the region. Further, bias_{ht} is the daily mean of the spatial deviation value.

$$STDM = \frac{\sum_{1}^{m} \mathrm{bias}_{ht}}{m}, \tag{5}$$

where m is the number of days of non-null bias_{ht} in the time series and STDM is the mean of the spatio-temporal deviation, which reflects the high-temperature value of the pixels in the time series relative to the overall region.

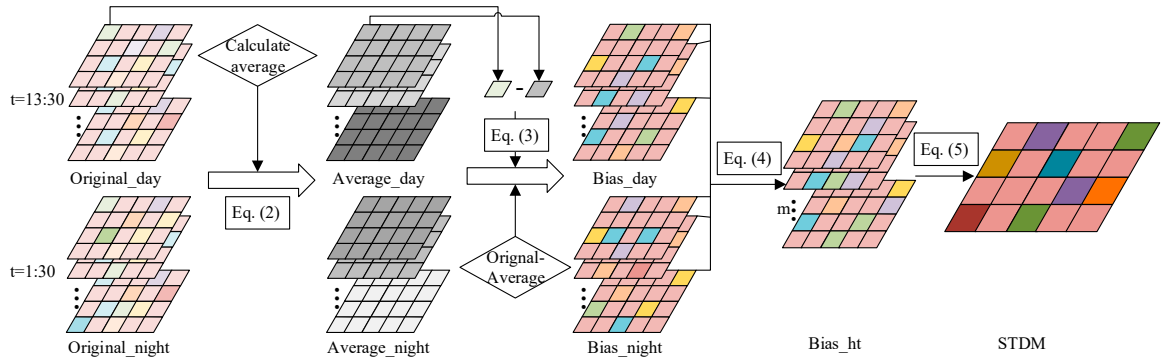


Figure 2. Flowchart of modeling process.

2.5. Regional High-Temperature Risk Classification

The STDM represents the deviation of each pixel from the mean temperature of the region. The standard deviation of the STDM (Equation (6)) is used to create a classification of the high-temperature risk. The criteria for this classification are shown in Table 3.

$$S = \sqrt{\frac{1}{m}\sum_{1}^{m}(x_{STMD} - \overline{x_{STMD}})^2}, \quad (6)$$

where x_{STMD} is the STDM value of the non-null pixels and $\overline{x_{STMD}}$ is the STDM mean of the non-null pixels, i.e., the regional average STDM.

Table 3. High-temperature risk classification.

Criteria for the Classification	Class
STDM > 2S	Highest average temperature
S < STDM <= 2S	Higher average temperature
-S <= STDM <= S	Average temperature
-2 S <= STDM < -S	Lower average temperature
-2 S < STDM	Lowest average temperature

3. Results

This paper first describes the temperature curve of the study area from 2003 to 2018, and grasps the development trend in the whole. After that, the multi-year STDM of the whole region, the single-year STDM of the year with high-temperature risk and the multi-year STDM of the city with high- temperature risk were calculated, and the comprehensive analysis was carried out in terms of the whole region, space, and time.

3.1. Trend of Temperature from 2003 to 2018

In order to explore the temporal and spatial variation of high-temperature risk in the Huang-Huai-Hai, we calculated the regional average near-high temperature mean, near-lowest temperature mean, and the combined high-temperature mean in the study area from July to August in 2003–2018, as shown in Figure 3. The trends of the near-highest mean and the near-lowest mean in the region are the same as the overall trends in the time series but there are some inconsistencies. For example, in 2013 when maize experienced strong heat damage, the near-highest temperature mean exhibited a low value, the peak value was observed for the near-lowest temperature, and the combined high-temperature mean reached a peak value. According to the agricultural meteorological disaster yearbook of all provinces and the high-temperature results of Liu [43], the degree of influence of high temperatures on maize heat damage in the Huang-Huai-Hai area was much higher in 2013 than in the adjacent years, and the high-temperature risk level was highest. Therefore, it is not comprehensive to use only the highest temperature data (i.e., data at 1:30 during the day). Since this is just the instantaneous temperature and weather conditions may be complex in the summer and many factors affect the temperature. So, the method proposed in this paper to combine the daytime and nighttime temperatures can better reflects the high-temperature conditions in the Huang-Huai-Hai area. The time-series variation of the average temperature in the Huang-Huai-Hai area indicates that the average temperature of the study area increased by 2.24 °C from 2003 and 2018 and the high-temperature risk increased significantly. The temperatures were significantly higher in 2005, 2013, 2017, and 2018 than in the adjacent years and in these years, extensive heat damage occurred in the Huang-Huai-Hai summer maize planting area.

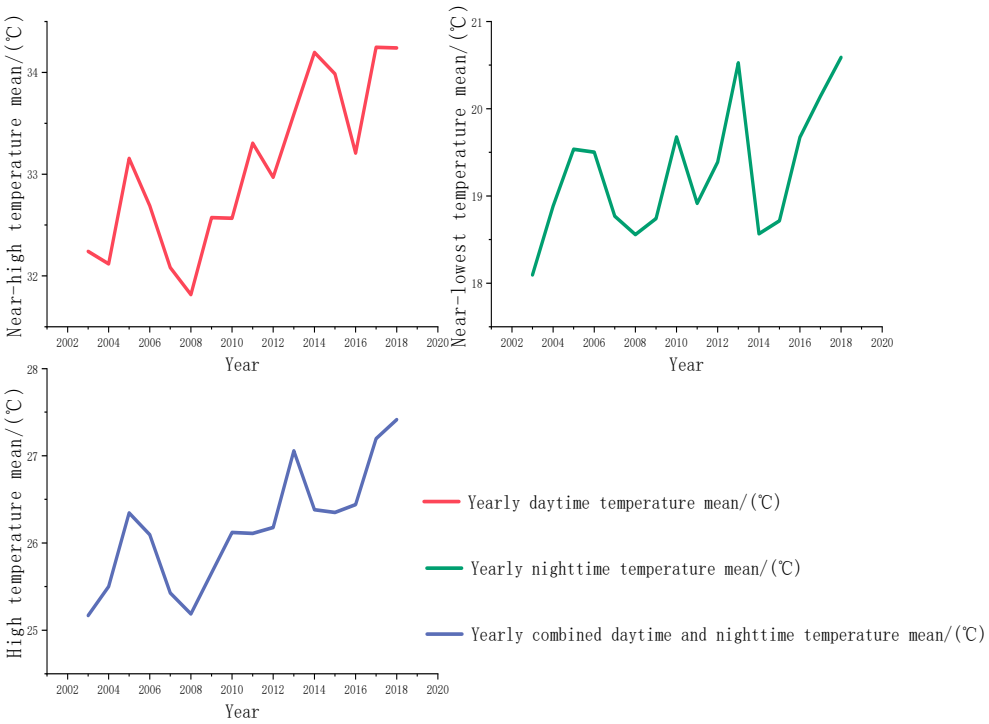


Figure 3. The trends of the mean values of the yearly daytime temperature, yearly nighttime temperature, and yearly combined daytime and nighttime temperature in 2003–2018.

3.2. Multi-Year STDM of the Whole Region

Overall, the spatial distribution of the whole Huang-Huai-Hai of STDM in July and August of 2003–2018 is shown in Figure 4. We can find that there is spatial heterogeneity in STDM within the study area. In Shijiazhuang City, Xingtai City, and Handan City in Hebei Province; Jiaozuo City, Luoyang City, Pingdingshan City, and Nanyang City in Henan Province; Fuyang City and Zhangzhou City in Anhui Province; Yuncheng City, Linfen City in Shanxi Province; and Weinan City, Xi'an City, Xianyang City and Baoji City in Shaanxi Province, the STDM values are relatively high, indicating that over the long term, these areas have a higher high-temperature risk than other areas in Huang-Huai-Hai. According to the provincial-level agro-meteorological monthly report issued by the China Weather Network and the meteorological data, the temperatures in these areas are consistently high in July and August and high-temperature events occur frequently. This result is also consistent with the results of Liu [43] regarding high-temperature risk zones. Yuncheng City, Linyi City, Weinan City, Xi'an City, and Xianyang City are relatively hot because these cities are located in relatively low-lying areas with strong atmospheric radiation and due to the leeward slope (north slope) of the Qinling Mountains, heat accumulates in these areas, resulting in high surface temperatures. It can be seen from Figure 4 that in the southwest of the study area, the STDM value is generally low due to high altitude. The STDM is higher in Xi'an, Weinan and Xianyang of Shaanxi where the altitude is lower. At the same time, the STDM value near the water body is lower, while the STDM value near the town is higher.

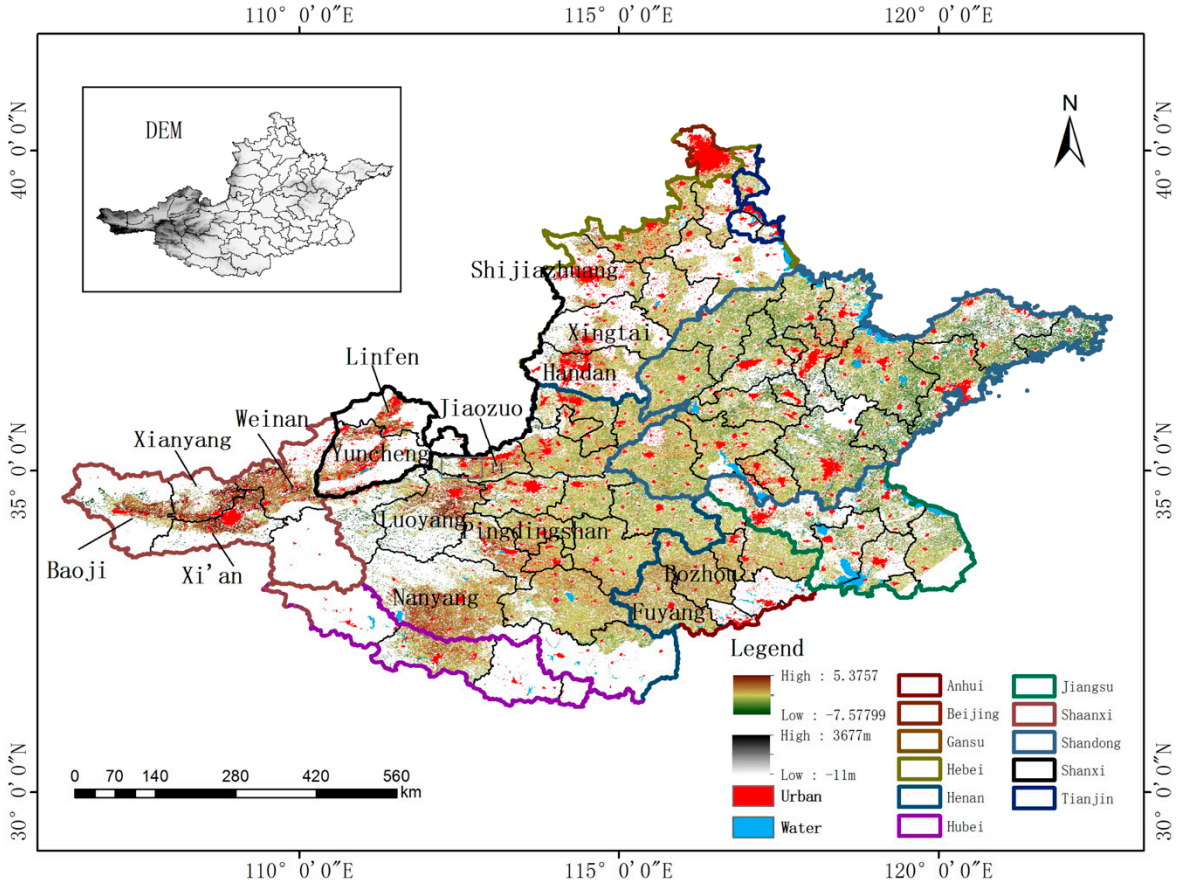


Figure 4. Spatial distribution of STDM (spatio-temporal deviation mean) in the Huang-Huai-Hai summer maize planting area in July and August of 2003–2018.

3.3. Single-Year STDM of the Year with High-Temperature Risk

In terms of space, the years with high temperatures and heat damage were 2005, 2013, 2017, and 2018. Therefore, we selected these years for focus analysis and classified them according to the classification method in Table 3. The results are shown in Figure 5.

In the four years of high-temperature events, the high-temperature risk was significantly higher in the south and northwest of the study area than in other regions and the regions with high-temperature risk were similar for the four years. These areas are mainly located in Xi'an and Weinan in Shaanxi Province, the southern part of Shanxi Province, the northwestern, southwestern, and central part of Henan Province, the northern part of Anhui Province, and some of the southwestern part of Hebei Province. According to the China Weather Net (2005), the temperatures in northern, central, and southwestern Henan were higher in 2005 than in previous years. According to the research results of Li [45], in 2013, the southern part of Huang-Huai-Hai experienced continuous high temperatures and most of the maize grown south of the Yellow River in Henan Province suffered from severe heat damage. According to the statistical yearbook of meteorological disasters in Anhui Province and Li [46], in 2013, northern Anhui suffered from extremely high temperatures and heat damage and the maize yield was relatively low. Zhu [47] found that in 2017, there was significant heat damage to maize in northwestern Henan. The average summer temperature in 2018 was the highest in nearly five years based on the major climate events in Anhui Province. According to the above existing studies and data, the spatial distribution of high temperatures and heat damage of crops in the Huang-Huai-Hai area are similar to those of the results that are shown in Figure 5. Therefore, the high temperature risk classification method specified in this study is reasonable.

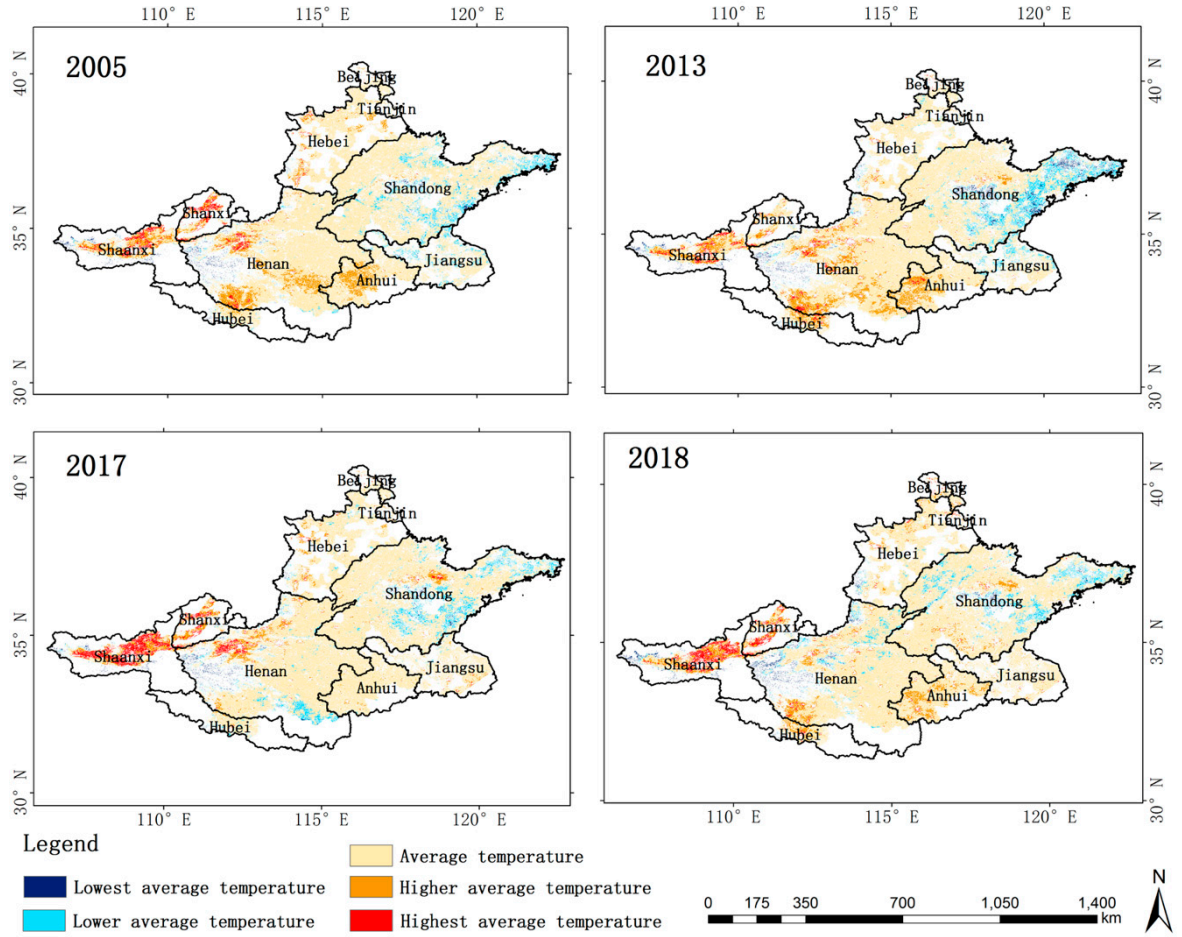


Figure 5. Spatial distribution of the spatio-temporal deviation mean (STDM) in July to August in years of high-temperature events.

3.4. Multi-Year STDM of the City with High-Temperature Risk

In terms of time, we analyzed the trend of high-temperature risk for many years in terms of cities. At the same time, in order to further analyze the high temperature risks, the standard deviation was used as the high-temperature risk threshold. The average value of the STDM in the cities in 2003–2018 was calculated to assess high-temperature risk. The annual temperature trend was analyzed, and three categories were established: Increasing high-temperature risk zone, stable zone, and decreasing high-temperature risk zone (Table 4).

Table 4. Categories of high-temperature risk zones.

Grade	Feature
Increasing high-temperature risk zone	Regional high-temperature risk value increases over time
Stable high-temperature risk zone	Regional high-temperature risk value is stable over time
Decreasing high-temperature risk zone	Regional high-temperature risk value decreases over time

Combined with Table 4 and Figure 6, we can find that the high-temperature risk values of Shijiazhuang City, Jiaozuo City, Weinan City, Xi'an City, and Xianyang City increase over time, so these cities belong to the increasing high-temperature risk zone. The high-temperature risk values of Xiangfan City, Yuncheng City, and Luoyang City exhibited no changes, and these cities were located in a zone of stable high-temperature risk. The high-temperature risk values of Handan City, Xingtai City, Zhangzhou City, Fuyang City, Nanyang City, Linfen City, and Pingdingshan City exhibited a downward trend over time, and these cities were in the decreasing high-temperature risk zone.

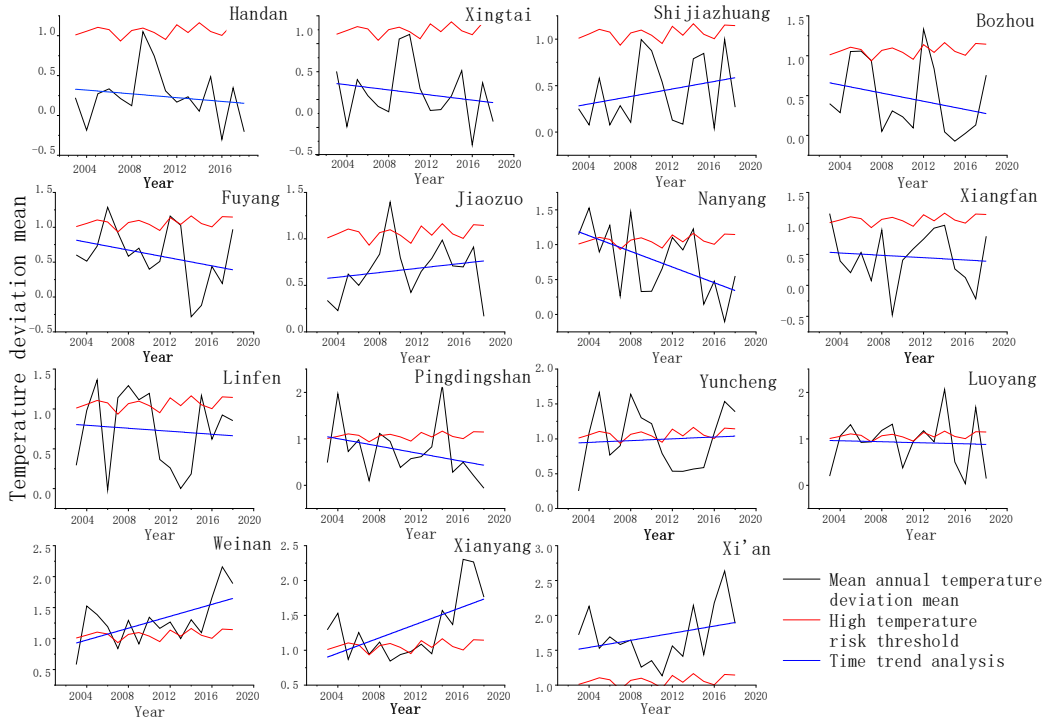


Figure 6. Trends of high-temperature risk over time in different cities.

In addition to the characterization of multi-year trends, we quantified the number of high-temperature risks in cities that exceeded the threshold. The results are shown in Figure 7. The results for these cities ranged from 0–16 times and the average was five times. We can find that the city where the high-temperature risk occurs relatively frequently is Linfen City, Luoyang City, Yuncheng City, Xianyang City, Weinan City, and Xi'an City. As shown in Figure 6, the temperature of Xianyang, Weinan and Xi'an keeps rising, which belong to the increasing high-temperature risk zone. Moreover, the three cities in Figure 7 exceed the threshold most frequently. Therefore, the probability of high-temperature risk in these cities is relatively high. Additionally, there should be a focus on the prevention of high-temperature risk in these cities.

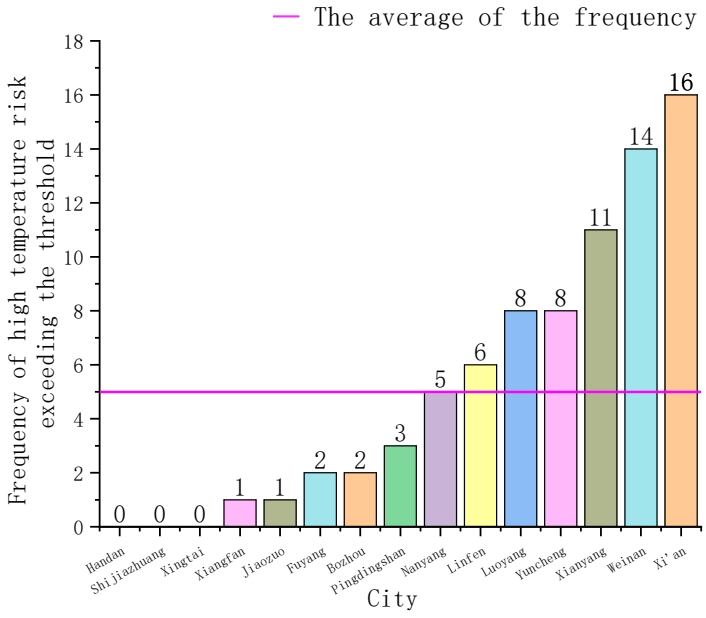


Figure 7. Occurrence and frequency of high-temperature risk in cities from 2003 to 2018.

4. Discussion

In this paper, the STDM high temperature risk assessment method is proposed by considering the temperature at night and day. Additionally, it is applied to the high temperature calculation of the Huang-Huai-Hai, and a reasonable high temperature spatial distribution is obtained. Compared with the high-temperature spatial distribution calculation of Liu [6] based meteorological point data, this paper takes remote sensing data as the data source, and the scale is more accurate, which can better reflect the high temperature of the block level. In addition, compared with Liu's method of using 34 °C as the high temperature threshold based on meteorological data, this paper proposes a method based on relative temperature value, which avoids the problem that it is difficult to determine the high temperature threshold based on remote sensing data, and comprehensively considers the overall temperature in the region, which is more suitable for the temperature characteristics of the research area itself. Moreover, the method for dynamically determining the threshold proposed in this paper is also applicable to the calculation of high temperature spatial distribution of other crops, not limited to maize.

Compared with the method that Liu used to calculate the local high temperature in the sliding window to reflect the relationship between each pixel and adjacent pixels [43], the method proposed in this paper comprehensively considered the temperature characteristics of each pixel and the whole region, and was more suitable for the calculation of the distribution of high temperature in a large range. In addition, Liu's article only uses the temperature during the day, without considering that the high temperature at night will also have an impact on maize. The method of this paper considers the temperature of day and night, which can calculate the temperature effect more accurately, and depict the spatial distribution of temperature.

The spatial resolution used in this study is 1 km, but there are a lot of mixed pixels in Huang-Huai-Hai. Therefore, in subsequent studies, higher resolution thermal infrared data should be used to calculate the surface temperature of specific crops and improve the accuracy of high-temperature risk assessment. Due to the large extent of summer maize in Huang-Huai-Hai Plain, there are considerable phenological differences during maize growth in different areas. We used a calendar period in this study, but in a future study, the phenological periods of each pixel should be used to assess the interactions between the growth periods and the high-temperature risk of maize. This will improve the assessment of high-temperature risk. This paper focuses on the spatial distribution of high temperature risk of maize. Since there are many factors affecting corn yield, this paper does not conduct an in-depth study on the relationship between STDM and corn yield. However, the high temperature and heat damage of maize is closely related to the yield. Therefore, in the follow-up studies, we will consider adding other factors and using non-linear methods to further study its relationship with yield [48], so as to provide support for better guidance of maize production.

5. Conclusions

Regional scale high temperature risk assessment is mainly based on remote sensing inversion temperature products (such as MODIS LST), but the generalization of such risk models is poor, because parameters such as the absolute high temperature threshold need to be continuously optimized according to different regions. In this study, a spatio-temporal temperature deviation model (STDM) was proposed to evaluate the relative high temperature risk of each space unit at a certain time or time period by calculating the difference between the average high temperature of each space unit at any time and the average high temperature of the study area. The results showed that this method could accurately express the high temperature risk during flowering period in the Huang-Huai-Hai summer maize region of China from 2003 to 2018, and no regional parameters such as temperature threshold were needed. It could be used as a new method to evaluate regional high temperature risk.

From 2003 to 2018, the summer temperature in the Huang-Huai-Hai summer maize region increased by 2.24 °C; the temperatures in the northwestern, southwestern, and southern parts were relatively high, and the area was classified as a zone of a stable high-temperature risk. At the urban

scale, cities in the zone of increasing high-temperature risk included Shijiazhuang City, Jiaozuo City, Weinan City, Xi'an City, and Xianyang City. Xiangfan City, Yuncheng City, and Luoyang City were located in the zone of stable high-temperature risk. Cities in the zone of decreasing high-temperature risk included Handan City, Xingtai City, Zhangzhou City, Fuyang City, Nanyang City, Linfen City, and Pingdingshan City.

Continued high temperature will affect the photosynthesis and reproductive function of maize, accelerate the process of fertility, greatly reduce the accumulation of dry matter, bulk density, quality and yield, and cause diseases in specific cases [2]. Luoyang City, Yuncheng City, Xianyang City, Weinan City, and Xi'an City were located in zones with a high probability of high-temperature risk and breed and promote heat-tolerant maize varieties and adjust the sowing date should be taken to avoid problems [2]. Cities located in zones of increasing and stable high-temperature risk should improve their risk prevention, awareness, and response. In addition, maize varieties resistant to high temperatures should be planted in these areas to achieve stable and sustainable maize production. Cities located in zones of increasing and stable high-temperature risk should appropriately reduce the planting density of field maize and timely irrigation and spraying of foliar fertilizers when high temperatures occur. In addition, high temperature resistant maize varieties should be grown in these areas to achieve stable and sustainable maize production.

Author Contributions: Conceptualization, S.L.; Methodology, Z.Z. and X.H.; Software, X.H.; Validation, L.Z. and X.H.; Formal analysis, L.Z. and X.H.; Investigation, L.Z.; Resources, Z.Z.; Data curation, X.H.; Writing—original draft preparation, X.H.; Writing—review and editing, L.Z. and Z.L; Visualization, L.Z.; Supervision, Z.L.; Project administration, X.Z.; Funding acquisition, X.Z.

Funding: This research was funded by the National Natural Science Foundation of China, grant number 41771104. We are also grateful to the China Scholarship Council for their help of their funding support.

Conflicts of Interest: The authors declare no conflict of interest.

References

1. Wang, W.; Yang, L.; Li, C.; Liu, H.; Jin, X. Effect of high temperature heat damage on summer maize production. *Barley Cereal Sci.* **2014**, 8–9. [CrossRef]
2. Chen, Z.; Wang, A.; Wang, J.; Xue, J.; Dong, X.; Wei, G. Influence of High Temperature on Growth and Development of Maize. *Crops* **2008**, *4*, 90–92.
3. Lu, W.; Yu, H.; Cao, S.; Chen, C. Effects of Climate Warming on Growth Process and Yield of Summer Maize in Huang-Huai-Hai Plain in Last 20 Years. *Sci. Agric. Sin.* **2015**, *48*, 3132–3145.
4. Sun, X.; Long, Z.; Song, G.; Chen, C. Effects of Climate Change on Cropping Pattern and Yield of Summer Maize-Winter Wheat in Huang-Huai-Hai Plain. *Sci. Agric. Sin.* **2017**, *50*, 2476–2487.
5. Zhang, L.; Liu, Z.; Liu, D.; Xiong, Q.; Yang, N.; Ren, T.; Zhang, C.; Zhang, X.; Li, S. Crop Mapping Based on Historical Samples and New Training Samples Generation in Heilongjiang Province, China. *Sustainability* **2019**, *11*, 5052. [CrossRef]
6. Liu, Z.; Qiao, H.; Zhao, Z.; Li, S.; Chen, Y.; Zhang, X. Spatial Distribution of High Temperature Stress at Corn Flowering Stage in Huang-Huai-Hai Plain of China. *Trans. Chin. Soc. Agric. Mach.* **2015**, *46*, 272–279.
7. He, L.; Wu, M.; Hou, Y.; Zhao, G.; Jin, N.; Yu, Q. Statistical characteristics of heat stress in early rice based on extreme value distribution in China. *Chin. J. Eco-Agric.* **2018**, *26*, 1601–1612.
8. Jiang, Z.; Wei, X.; Jiang, H. Monitoring the land surface temperature using MODIS data in Zhejiang of China. In Proceedings of the 2011 19th International Conference on Geoinformatics, Shanghai, China, 24–26 June 2011; pp. 1–6.
9. Benali, A.; Carvalho, A.C.; Nunes, J.P.; Carvalhais, N.; Santos, A. Estimating air surface temperature in Portugal using MODIS LST data. *Remote Sens. Environ.* **2012**, *124*, 108–121. [CrossRef]
10. McMillin, L.M. Estimation of sea surface temperatures from two infrared window measurements with different absorption. *J. Geophys. Res.* **1975**, *80*, 5113–5117. [CrossRef]
11. Jimenez-Munoz, J.; Sobrino, J.A. Split-Window Coefficients for Land Surface Temperature Retrieval from Low-Resolution Thermal Infrared Sensors. *IEEE Geosci. Remote Sens. Lett.* **2008**, *5*, 806–809. [CrossRef]

12. Wan, Z.; Dozier, J. A generalized split-window algorithm for retrieving land-surface temperature from space. *IEEE Trans. Geosci. Remote Sens.* **1996**, *34*, 892–905.
13. Wan, Z.; Zhang, Y.; Zhang, Q.; Li, Z. Validation of the land-surface temperature products retrieved from Terra Moderate Resolution Imaging Spectroradiometer data. *Remote Sens. Environ.* **2002**, *83*, 163–180. [CrossRef]
14. Salisbury, J.W.; D'Aria, D.M. Emissivity of terrestrial materials in the 8–14 µm atmospheric window. *Remote Sens. Environ.* **1992**, *42*, 83–106. [CrossRef]
15. Ri, C.; Liu, Q.H.; Li, H. Improved split window algorithm to retrieve LST from Terra /MODIS data. *J. Remote Sens.* **2013**, *17*, 830–840.
16. Wang, S.; He, L. Practical split-window algorithm for retrieving land surface temperature over agricultural areas from ASTER data. *J. Appl. Remote Sens.* **2014**, *8*, 083582. [CrossRef]
17. Metz, M.; Andreo, V.; Neteler, M. A New Fully Gap-Free Time Series of Land Surface Temperature from MODIS LST Data. *Remote Sens.* **2017**, *9*, 1333. [CrossRef]
18. Westermann, S.; Langer, M.; Boike, J. Spatial and temporal variations of summer surface temperatures of high-arctic tundra on Svalbard—Implications for MODIS LST based permafrost monitoring. *Remote Sens. Environ.* **2011**, *115*, 908–922. [CrossRef]
19. Zhu, W.; Lű, A.; Jia, S. Estimation of daily maximum and minimum air temperature using MODIS land surface temperature products. *Remote Sens. Environ.* **2013**, *130*, 62–73. [CrossRef]
20. Huang, R.; Zhang, C.; Huang, J.; Zhu, D.; Wang, L.; Liu, J. Mapping of Daily Mean Air Temperature in Agricultural Regions Using Daytime and Nighttime Land Surface Temperatures Derived from TERRA and AQUA MODIS Data. *Remote Sens.* **2015**, *7*, 8728–8756. [CrossRef]
21. Zeng, L.; Wardlow, B.; Tadesse, T.; Shan, J.; Hayes, M.; Li, D.; Xiang, D. Estimation of Daily Air Temperature Based on MODIS Land Surface Temperature Products over the Corn Belt in the US. *Remote Sens.* **2015**, *7*, 951–970. [CrossRef]
22. Carter, E.K.; Melkonian, J.; Riha, S.J.; Shaw, S.B. Separating heat stress from moisture stress: Analyzing yield response to high temperature in irrigated maize. *Environ. Res. Lett.* **2016**, *11*, 94012. [CrossRef]
23. Butler, E.E.; Huybers, P. Adaptation of US maize to temperature variations. *Nat. Clim. Chang.* **2013**, *3*, 68–72. [CrossRef]
24. Muro, J.; Strauch, A.; Heinemann, S.; Steinbach, S.; Thonfeld, F.; Waske, B.; Diekkrüger, B. Land surface temperature trends as indicator of land use changes in wetlands. *Int. J. Appl. Earth Obs.* **2018**, *70*, 62–71. [CrossRef]
25. Williamson, S.; Hik, D.; Gamon, J.; Kavanaugh, J.; Flowers, G. Estimating Temperature Fields from MODIS Land Surface Temperature and Air Temperature Observations in a Sub-Arctic Alpine Environment. *Remote Sens.* **2014**, *6*, 946–963. [CrossRef]
26. Renata, D. Difference in Canopy and Air Temperature as an Indicator of Grassland Water Stress. *Soil Water Res.* **2013**, *1*, 127–138. [CrossRef]
27. Huang, J.; Ma, H.; Fernando, S.; Phillip, L.; Liang, S.; Wu, Q.; Su, W.; Zhang, X.; Zhu, D. Evaluation of regional estimates of winter wheat yield by assimilating three remotely sensed reflectance datasets into the coupled WOFOST–PROSAIL model. *Eur. J. Agron.* **2019**, *102*, 1–13. [CrossRef]
28. Vancutsem, C.; Ceccato, P.; Dinku, T.; Connor, S.J. Evaluation of MODIS land surface temperature data to estimate air temperature in different ecosystems over Africa. *Remote Sens. Environ.* **2010**, *114*, 449–465. [CrossRef]
29. Cross, H.Z. Diallel Analysis of Duration and Rate of Grain Filling of Seven Inbred Lines of Corn. *Crop Sci.* **1975**, *15*, 532–535. [CrossRef]
30. Zhou, J.B.; Yang, G.H.; Sun, S.X.; Zhao, J.R. Current Situation and Prospect of Maize Production in the Huanghuaihai Summer Maize Region. *Crops* **2008**, *2*, 4–7.
31. Guo, Q.F.; Gao, X.X.; Liu, Q.; Liu, T.S.; Zhang, C.H.; Dong, R.; Ye, J.C. Maize Breeding Actualities and Innovation in Huanghe-Huaihe River Area. *J. Maize Sci.* **2007**, *6*, 1–4.
32. Yue, Y.; Zhao, W.; Zhou, X. Climatic Characteristics and Breeding Research Direction of Summer Maize in Huanghuaihai Region. *Agric. Technol.* **2009**, *29*, 28–30.
33. Caetano, M.; Araujo, A. Comparing Land Cover Products CLC2000 and MOD12Q1 for Portugal. *Global Developments in Environmental Earth Orbservation from Space*. 2006, pp. 469–477. Available online: https://www.researchgate.net/publication/239600644_Comparing_land_cover_products_CLC2000_and_MOD12Q1_for_Portugal (accessed on 21 November 2019).

34. Mao, J.; Thornton, P.E.; Shi, X.; Zhao, M.; Post, W.M. Remote Sensing Evaluation of CLM4 GPP for the Period 2000–2009. *J. Clim.* **2012**, *25*, 5327–5342. [CrossRef]
35. Naveed, S.; Aslam, M.; Maqbool, M.A.; Bano, S.; Zaman, Q.U.; Ahmad, R.M. Physiology of high temperature stress tolerance at reproductive stages in maize. *Anim. Plant Sci.* **2014**, *24*, 1141–1145.
36. Dupuis, I.; Dumas, C. Influence of temperature stress on in vitro fertilization and heat shock protein synthesis in maize (*Zea mays* L.) reproductive tissues. *Plant Physiol.* **1990**, *94*, 665–670. [CrossRef]
37. Hatfield, J.L.; Prueger, J.H. Temperature extremes: Effect on plant growth and development. *Weather Clim. Extrem.* **2015**, *10*, 4–10. [CrossRef]
38. Badu-Apraku, B.; Hunter, R.B.; Tollenaar, M. Effect of temperature during grain filling on whole plant and grain yield in maize (*Zea mays* L.). *Can. J. Plant Sci.* **1983**, *63*, 357–363. [CrossRef]
39. Yang, H.; Huang, T.; Ding, M.; Lu, D.; Lu, W. High Temperature during Grain Filling Impacts on Leaf Senescence in Waxy Maize. *Agron. J.* **2017**, *109*, 906. [CrossRef]
40. Wan, Z. New refinements and validation of the collection-6 MODIS land-surface temperature/emissivity product. *Remote Sens. Environ.* **2014**, *140*, 36–45. [CrossRef]
41. Yao, X.; Mokbel, M.; Ye, S.; Li, G.; Alarabi, L.; Eldawy, A.; Zhao, Z.; Zhao, L.; Zhu, D. LandQv2: A MapReduce-Based System for Processing Arable Land Quality Big Data. *ISPRS Int. J. Geo-Inf.* **2018**, *7*, 271. [CrossRef]
42. Peters, D.B.; Pendleton, J.W.; Hageman, R.H.; Brown, C.M. Effect of Night Air Temperature on Grain Yield of Corn, Wheat, and Soybeans. *Agron. J.* **1971**, *63*, 809. [CrossRef]
43. Liu, Z.; Wang, X.; Liu, D.; Zan, X.; Zhao, Z.; Li, S.; Zhang, X. Spatial distribution of high temperature risk on summer maize in Huang-huai-hai Plain based on MODIS data. *Trans. Chin. Soc. Agric. Eng.* **2018**, *34*, 175–181.
44. Tollenaar, M.; Bruulsema, T.W. Effects of temperature on rate and duration of kernel dry matter accumulation of maize. *Can. J. Plant Sci.* **1988**, *68*, 935–940. [CrossRef]
45. Investigation Report on Maize Disaster in Huang-Huai-Hai Area in 2013. Available online: http://chinamaize.blog.sohu.com/279855167.html (accessed on 21 November 2019).
46. Li, D.A. Occurrence and countermeasures of high temperature heat damage in summer maize production in central and western regions of Huaibei in 2013. *Mod. Agric. Sci. Technol.* **2014**, 63–65. [CrossRef]
47. Zhu, B.M.; Zhou, Q.; Wu, Z.X.; Zhang, P.; Si, H.; Yang, Y.J. Analysis of Meteorological Causes to Influence Differentiation Abnormity of Female Ears in Summer Corn in Northwestern Shandong in 2017. *Guizhou Agric. Sci.* **2018**, *46*, 50–54.
48. Zhu, P.; Zhuang, Q.; Archontoulis, S.V.; Bernacchi, C.; Müller, C. Dissecting the nonlinear response of maize yield to high temperature stress with model-data integration. *Glob. Chang. Biol.* **2019**. [CrossRef]



© 2019 by the authors. Licensee MDPI, Basel, Switzerland. This article is an open access article distributed under the terms and conditions of the Creative Commons Attribution (CC BY) license (http://creativecommons.org/licenses/by/4.0/).